Transactions, **SMiRT-26**
Berlin/Potsdam, Germany, July 10-15, 2022
Special session: Impact tests and numerical analyses

BENDING DAMAGE OF REINFORCED CONCRETE SLABS SUBJECTED TO SOFT MISSILE IMPACT, PART I: RECENT TESTS ON INFLUENCE OF INCLINED IMPACT

Ari Vepsä[1], Anthony Darraba[2], Alexis Fedoroff[1], Christian Heckötter[3], Shohei Sawada[4], Christian Schneeberger[5], Francois Tarallo[6]

[1] Senior Scientist, VTT Technical Research Centre of Finland, Espoo, Finland (Ari.Vepsa@vtt.fi)
[2] Structural Engineer, Électricité de France (EDF), Lyon, France
[3] Technical Expert, Gesellschaft für Anlagen- und Reaktorsicherheit (GRS) gGmbH, Cologne, Germany
[4] Senior Engineer, Kajima Corporation, Tokyo, Japan
[5] Deputy Section Head, Swiss Federal Nuclear Safety Inspectorate ENSI, Brugg, Switzerland
[6] Civil Engineer - Senior Expert, Institut de Radioprotection et de Sûreté Nucléaire IRSN, Fontenay- aux-Roses, France

ABSTRACT

A series of soft impact tests were carried out with square reinforced concrete slabs positioned in an inclined angle in relation to the impacting projectile. The projectile used in the tests was a hollow steel tube weighing 50 kg. The purpose of the tests was to study the effect of the inclination angle to the response of the slabs. The inclination angle that resulted the projectile to slide on the impacted surface was between 10° and 20°. Reduced normal component of the loading combined with sliding and rotation of the projectile resulted remarkable decrease in the level of target response in the tests with 20° inclination angle. The target response in the tests with 10° inclination angle was even slightly higher than in the perpendicular impact tests that were used for comparison.

INTRODUCTION

Impact of a soft projectile, like a fuselage of an aircraft, is one possible threat for the safe operation of nuclear power plants. Testing of reinforced concrete (rc) structures against different types of impact loading has been carried out at VTT in a series of jointly funded international projects called IMPACT since 2005. Soft impact testing has been an essential part of these projects (Tarallo and Rambach, 2013). One of the main purposes of these soft impact tests has been to act as reference data against which computational models can be validated. In all the previous tests, the impacts have been perpendicular to the plane of the impacted slab. Recently, a series of four inclined-impact tests was carried out to complement the study of soft impact. The main interest lies in the effect of the inclination angle on the displacements and strains, at which angle the projectile begins to slide on the target surface and what could be the friction coefficient between the projectile and the target. Two so-called force-plate tests were carried out with inclination angles of 10° and 20° to accompany the slab tests. The purpose of the force-plate tests was to obtain understanding about the impact force affecting the slab in this type of tests.

METHODS

All the tests discussed in this paper were carried out with VTT impact test apparatus (Vepsä et al., 2011). All slabs were 150 mm thick and simply supported on four edges with in-plane dimensions of 2.1x2.1 m and a span width of 2 m in both directions. The slabs were longitudinally reinforced using Ø6 mm rebars

with spacing of 50 mm each way and each face with the concrete cover of 15 mm. The slabs had shear reinforcement in a form of closed Ø6 mm stirrups with spacing of 200 mm in one and 50 mm in the other direction. The rebar steel was A500HW for reference test slabs TF11 and TF12 and B500B steel for slabs IB1-IB4. The projectiles, each weighing about 50 kg, were made of D_o254 mm and t2 mm stainless steel (EN 1.4432) pipe with a t3 mm dome of the same material welded at the front. The impacts took place against the slab surface which was facing upwards when cast. This surface was not as smooth as the opposite surface facing the casting formwork, resulting in an increase in the friction between the surface and the impacting projectile.

The slabs were cast with a concrete mix having a nominal strength of C40/K50 with the maximum aggregate size of 8 mm. Slabs IB1 – IB4 were cast using the same batch of concrete but tested at very different times (30 – 200 days after casting). The mechanical properties of concrete change during this period. The basic test parameters of the included tests are listed in Table 1. Four so-called force-plate tests are included (FP4, FP8, FPI1, FPI2). The table includes also basic mechanical properties of concrete like unconfined compression strength, f_c, splitting tensile strength, f_{ct}, and Young's modulus, E_c. The values for slabs TF11 and TF12 were obtained with cylinders of size D 150 mm and h 300 mm while D100*h200 mm cylinders were used in connection with slabs IB1 - IB4.

Table 1: Test parameters (v_0 impact velocity, α inclination angle, m_p, projectile mass, E_k kinetic energy, v_{0n} normal component of the impact velocity, E_{kn} normal component of the kinetic energy) for experiments on bending damage (tests [a] IMPACT II tests (Tarallo and Rambach, (2013)), [b] latest tests from IMPACT IV/NEREID project, [c] test from SAFIR project).

Test	α / °	m_p	v_0	E_k	v_{0n}	E_{kn}	f_c	f_{ct}	E_c
	°	kg	m/s	kJ	m/s	kJ	MPa	MPa	GPa
FP4[a]	0	50.1	137.7	475	137.7	475			
FP8[a]	0	50.1	102.2	261.6	102.2	261.6			
FPI1[b]	20	50.18	114.5	328.9	107.6	290.5			
FPI2[c]	10	49.72	113	317.4	111.3	307.9			
TF 11[a]	0	50.5	108.3	296.2	108.3	296.2	56	3.51	28.16
TF 12[a]	0	50.1	130.2	424.6	130.2	424.6	60.7	4.47	29.87
IB1[b]	20	49.92	111.8	312	105.1	275.5	48.3	3.8	29.3
IB2[b]	10	50.04	112.9	318.9	111.2	309.3	56.8	-	30.2
IB3[b]	20	50.12	128.4	413.2	120.7	364.8	56	-	28.7
IB4[b]	10	49.54	130	418.6	128	406	58.4	4.1	28.9

The tested slabs were equipped with strain gauges, glued on the reinforcement bars, as well as displacement sensors, placed on the rear surface of the slabs. In addition, support forces were measured both on the supports acting in the impact direction as well as those acting in the transverse direction. The tests were documented with two high-speed video cameras. One of the cameras was located on top of the slab while the other took footage from an oblique right perspective. Kinematic analysis was carried out for the impacts using the footage taken from top of the slab.

Extensive set of mechanical tests was carried out for the materials used for construction of the projectile and the slabs IB1-IB4. The reinforcement used for the slabs was subjected to basic tensile testing, the results of which are presented in Table 2. The missile material was tested for tensile properties using digital image correlation technique. The resulting engineering as well as true stress–strain curves are plotted in Figure 1. The initial gauge length of 50 mm was used for determination of the engineering values. In addition to basic mechanical properties shown in Table 1, the batch of concrete IB1 – IB4 was subjected for more extensive testing. The results of these extensive tests are collected in Table 3. The parameters E_0 and n in Table 3 are used when defining the Young's (secant) modulus of concrete at different values of axial strain, ε, as follows:

$$E_c = E_0 e^{n\varepsilon}. \tag{1}$$

Table 2: Material parameters for the reinforcement used in slabs TF11, TF12 and IB1- IB4 ($R_{p0.2}$ – yield strength, R_m – ultimate strength, A_{10}/A_{100} ultimate elongation, A_{gt} total elongation under maximum load, E Young's modulus)

Test	$R_{p0,2}$	R_m	A_{10}/A_{100}	A_{gt}	E
	N/mm²	N/mm²	%	%	GPa
TF11	623.3	694.0	12.5	4.7	-
TF12	570.0	672.3	17.6	10.8	-
IB1-4*	634.8	714.5	9.0	-	191.92
IB1-4**	638.1	710.9	12.8	-	197.85
* With loading speed of 1.5 mm/min					
** With loading speed of 450 mm/min					

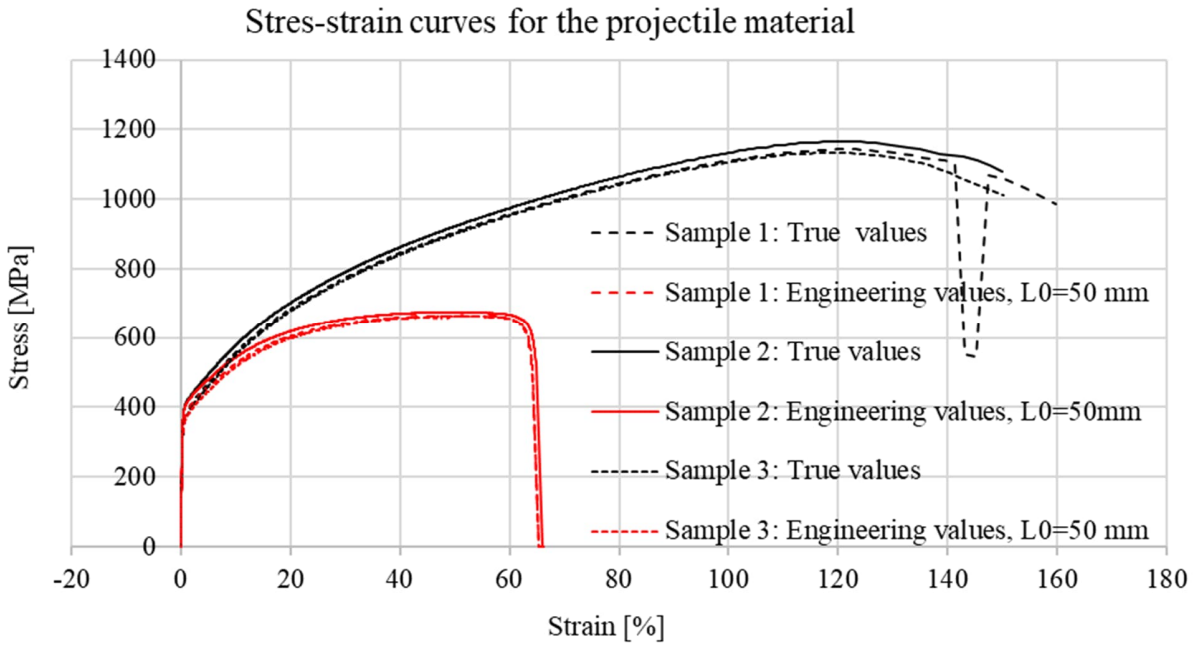

Figure 1: Stress-strain curves for the projectile material.

Table 3: Additional material parameters for the concrete used in tests IB1- IB4. (f_{cD} -unconfined compression strength, displacement driven, ε_m – strain at maximum load, ε_f – strain at failure $0.1f_c$, E_0 amplitude of the secant modulus curve while Loading (L) and Unloading (UL), n exponent of the secant modulus curve, ν Poisson's ratio, f_{ctm} – tensile strength from 3-point bending tests and G_f fracture energy from 3-point bending tests.)

Test	f_c	ε_m	ε_f	E_0 (L/UL)	n (L/UL)	ν	f_{ctm}	G_f
	MPa	%	%	GPa	-	-	MPa	N/m
IB1	45.6	0.3	0.9	27.688/74.551	2.998/-2.711	0.2	3.3	124
IB2	-	-	-	-	-	0.19	-	-
IB3	-	-	-	-	-	0.19	-	-
IB4	55.0	0.4	1.3	29.872/52.116	-3.187/-2.443	0.18	3.64	136

RESULTS

The graph on the right in Figure 2 shows the theoretical impact forces generated in a perpendicular impact as computed using Riera formula (Riera, 1968). The difference to a loading function caused by a real aircraft fuselage is the relatively large contribution of the crushing strength, P_c, to the total force. This contribution is emphasized as the impact velocity decreases. The very short part at the beginning of the curves is due to the projectile's front dome, having 3 mm wall thickness.

The forces measured during the impact in the force plate tests are shown on the left in Figure 2. The data shown is a 25 point (0.0244 ms) rolling average of the measured values. The higher impact velocity in test FP4 manifests itself as longer impact duration compared to the other tests. It has also marginally higher magnitude from the beginning of the impact. In general, the measured peak forces are relatively similar in each test up until roughly 7 ms, after which the force level in the inclined impact tests decreases more rapidly than in the other tests. The effect of the projectile's dome cannot be seen. This is most probably due to relatively insensitive measurement system

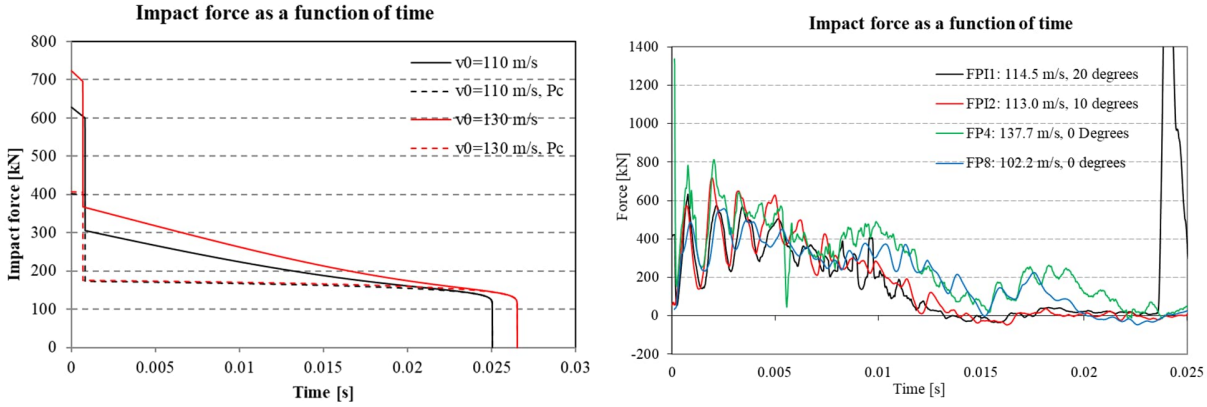

Figure 2. Impact force as a function of time computed using Riera formula (left) and the ones measured in the force plate tests (right).

The static friction angle and the minimum target angle to initiate projectile sliding were measured by sliding a tested projectile on the steely force plate (as such and sandblasted). The measured friction angles were 15.4° and 12.4° while the minimum angles to initiate sliding were 17.1° and 13.6°.

In the tests with inclination angle of 20° (IB1 & IB3), the projectile tended to slide along the impact surface with increased rotation towards the end of the impact. This finally led to the heavy rear part of the projectile hitting the target. When the inclination angle was reduced to 10°, the friction between the projectile and the target prevented this sliding from happening and the projectile behaviour was like that observed in a perpendicular angle impact. Photos taken above the slab at the different stages of impact in tests IB1 and IB2 are presented in Figure 3.

Figure 3. Top view of the impact in tests IB1 (top) and IB2 (bottom). Time moments: frame 1: 0 ms; frame 2: 3.7 – 3.75 ms, frame 3: 7.4 – 7.5 ms and frame 4: 11.1 – 11.3 ms.

Due to sliding, part of the total kinetic energy of the projectile at the moment of impact does not transfer to the slab and thus the damage caused to it remains smaller than in tests without sliding. The graph on the left in Figure 4 shows the kinetic energies, E_k, of the projectiles in tests IB1 and IB2 divided into components of sliding and projectile shortening. The same information is presented for tests IB3 and IB4 in the graph on the right. As can be seen, almost all of the initial kinetic energy of the projectile is spent on its shortening during the impact in tests with inclination angle of 10°. When the angle is increased to 20°, part of it goes to sliding and rotation of the projectile.

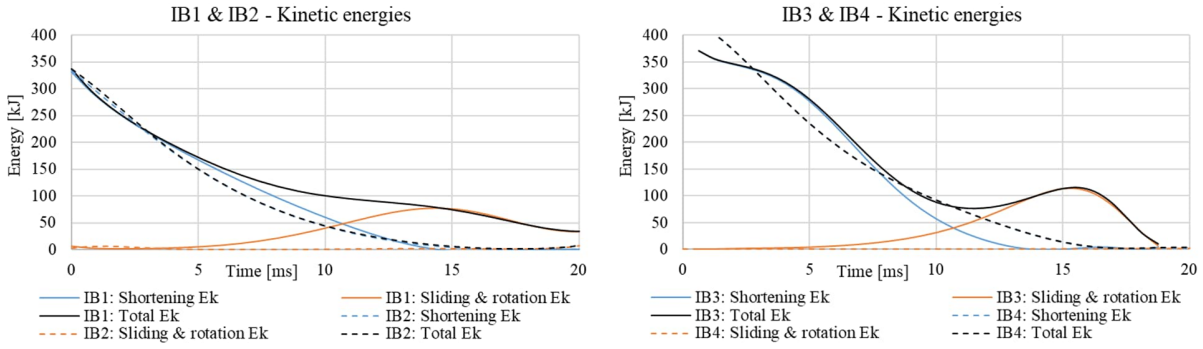

Figure 4. Projectile kinetic energies, E_k, in tests IB1 and IB2 (left) and IB3 and IB4 (right) divided into sliding and projectile shortening energies.

The front surfaces of the slabs IB3 and IB4 are shown in Figure 5 after the tests. The photographs show the sliding marks of the projectile in the 20° inclination angle test slabs IB3 as well as the point where the tail of the projectile has hit the target. Both of these marks are missing from the 10° inclination angle test slab IB4 as the angle becomes too small for sliding to happen. The same difference applies also for slabs IB1 and IB2. The projectiles used in tests TF12, IB3 and IB4 are shown in Figure 6. The folded front part of the projectile becomes tilted even in a perpendicular impact when the number of folds becomes large enough. This can be seen when comparing the projectiles used in tests TF12 and IB4 with 0° and 10° inclination angles.

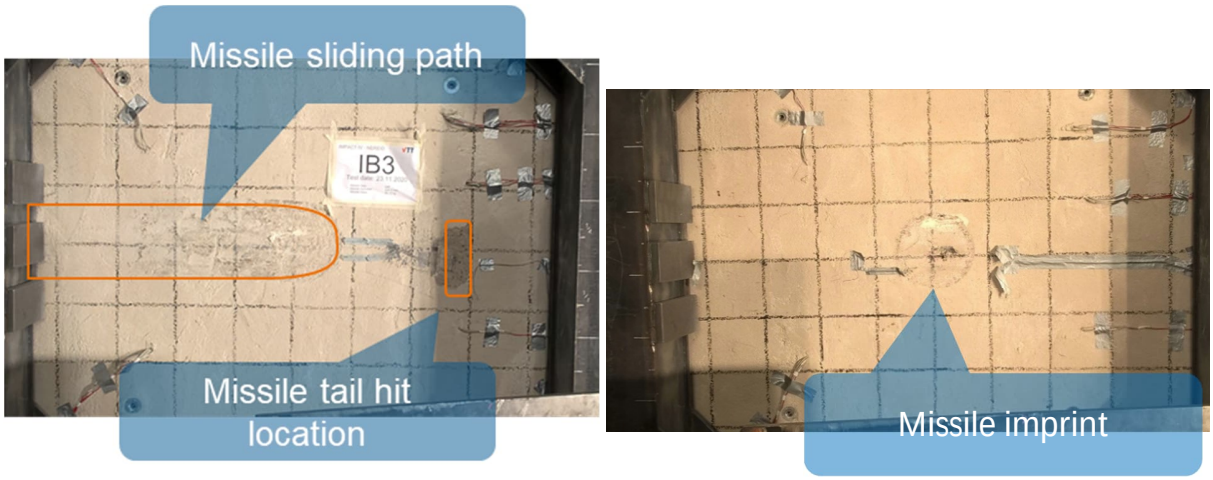

Figure 5. Front side of the target slab IB3 (left) and IB4 (right).

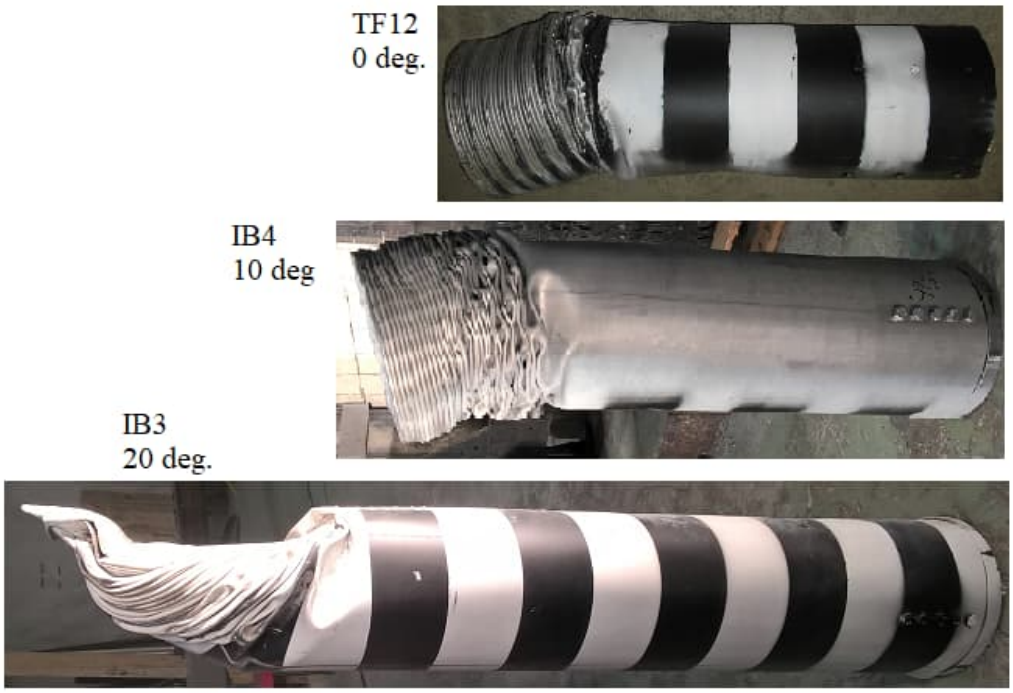

Figure 6. The projectiles used in tests TF12, IB3 and IB4 after the test.

The measurement results were in line with the ones obtained in the perpendicular-impact tests, accounting for the impact velocity component perpendicular to the slab surface and the side where the values were measured. In each test IB1 – IB4, the maximum displacements measured on the side of the projectile sliding (from here on slide side) were larger than on the other (non-slide) side. The comparison was carried out using 4 pairs of sensor locations. The difference was the largest in test IB3 (20°, 130 m/s) where the slide side values were on average 21 % larger than on the non-slide side. The difference was the lowest (9.1 – 9.2 % on average) in the tests with 10° inclination angle.

Increasing the inclination angle from 10° to 20°, and thus initiating sliding of the projectile, decreased the maximum displacements 26 % on average across 11 sensors with both impact velocities. Increasing the inclination angle from 0° to 10° increased the maximum displacements 3 % on average on the non-slide side and 11 % on the slide with the lower impact velocity. With the higher impact velocity, the corresponding values were 17 - 31 %. Part of the increase observed with the higher velocity can be attributed to higher strength of concrete in test TF12 than in test IB4. The maximum displacements obtained with each sensor are presented in Figure 7.

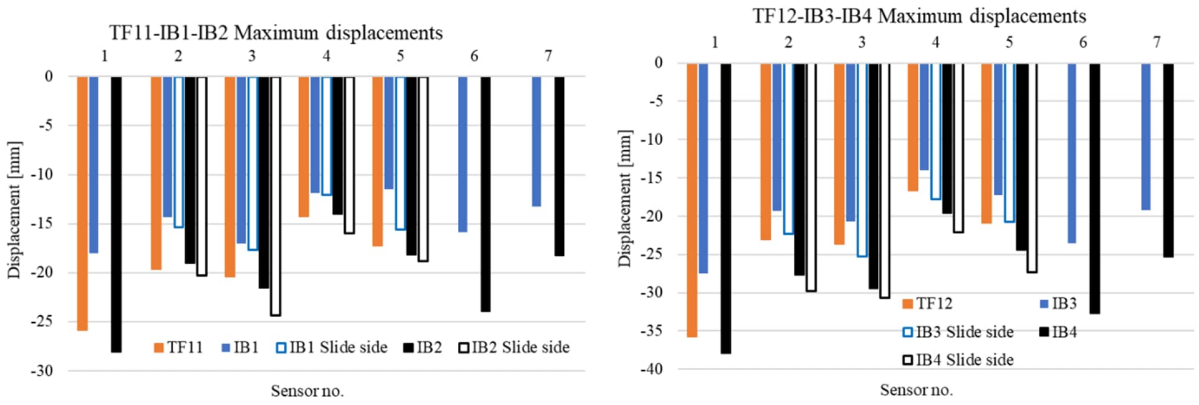

Figure 7. Maximum displacements of the tested slabs. Left: Lower velocity tests TF11, IB1 and IB2. Right: Higher velocity tests TF12, IB3 and IB4.

The displacements measured at the centre of the slab are presented in Figure 8 as a function of time. The results from tests with the lower impact velocity are shown on the left and the ones obtained with the higher impact velocity on the right. It can be seen how the displacement amplitudes in the tests with 0° and 10° inclination angle are very similar while those obtained in the tests with 20° inclination angle are much lower. It should be noted that in the case of 20° inclination angle (tests IB1 & IB3), the second displacement peak is as high as the first one or even higher. This can be attributed to the projectile's heavy tail hitting the target after the first peak. These secondary peaks are counted when determining the maximum values.

The displacements measured at different sides of the slabs 200 mm and 400 mm away from its centre point are presented in Figure 9 for the lower impact velocity tests and in Figure 10 for the higher impact velocity tests. The dashed lines represent the results measured on the slide side of the slab. X marks the horizontal co-ordinate of the sensor with respect to the centre point and Y the vertical co-ordinate when the slab is viewed from the front.

The reinforcement strains confirm the observations made from the measured displacements. In general, the highest response was achieved with 10° and the lowest with 20° inclination angle. The response was higher on the slide side than on the other side. Majority of the strain measurements failed in test IB1 with only 3 gauges providing reliable results. The measured rear surface horizontal reinforcement strains

at the centre of the slab in tests with the higher impact velocity are shown on the right in Figure 11. The locations of the gauges are shown on the left in the same figure.

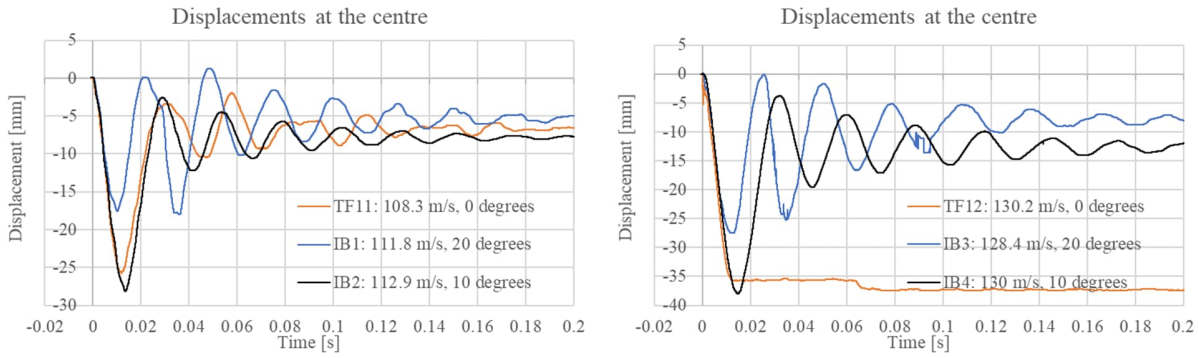

Figure 8. Displacements of the slab centre point. Left: Lower velocity tests TF11, IB1 and IB2. Right: Higher velocity tests TF12, IB3 and IB4.

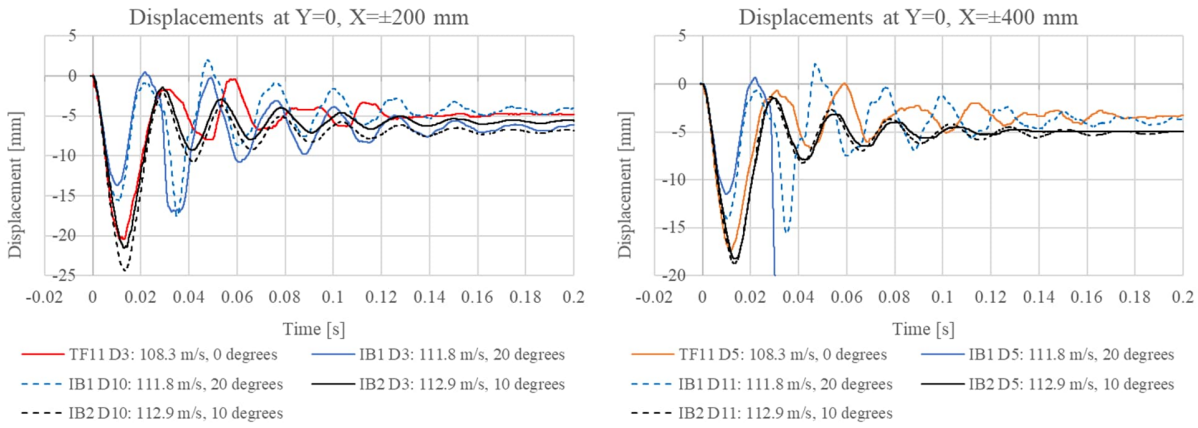

Figure 9. Displacements at Y=0, X=±200 (left) and Y=0, X=±400 (right) in tests IB1 and IB2.

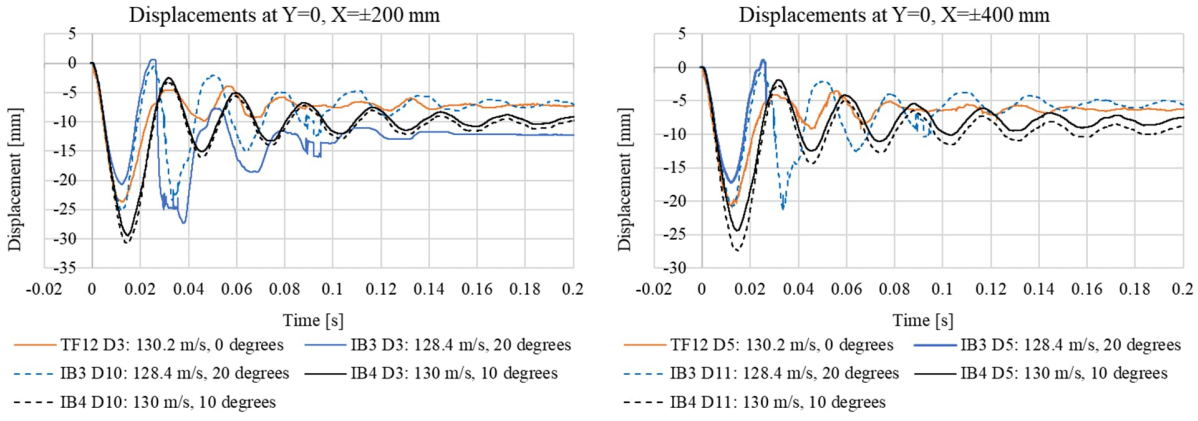

Figure 10. Displacements at Y=0, X=±200 (left) and Y=0, X=±400 (right) in tests IB3 and IB4.

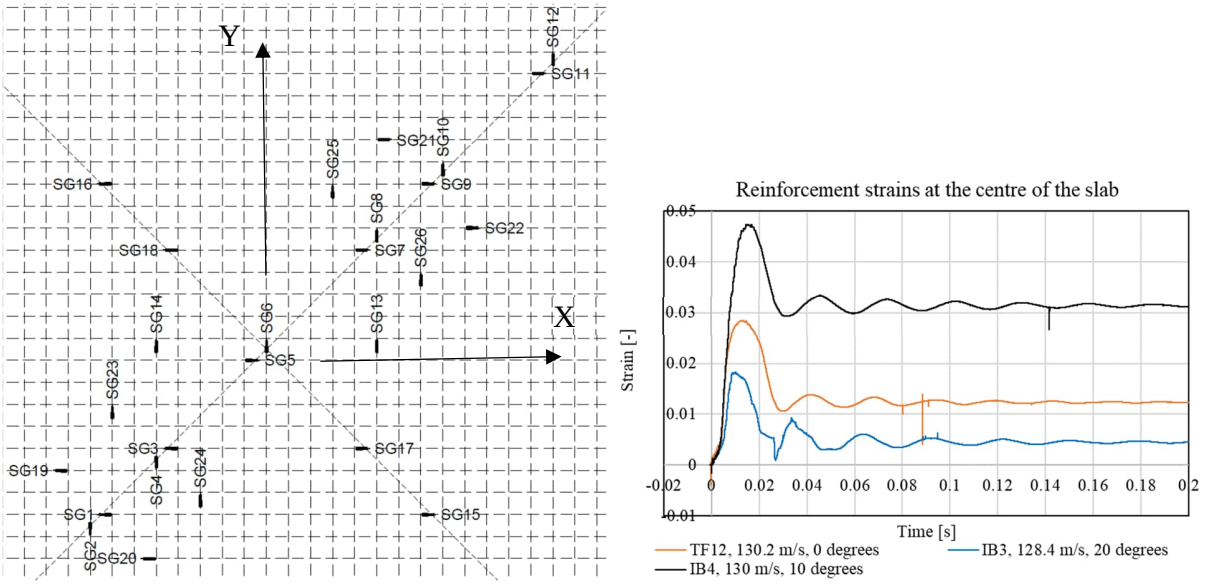

Figure 11. Left: Locations of the strain gauges. Right: Rear surface horizontal reinforcement strains at the centre of the slab (X=-40 mm, Y=25 mm).

The strains on the rear surface horizontal reinforcement at X=±210 mm and Y=±225 mm are presented in Figure 12 for the higher velocity tests. The strains were measured at every four quartiles of the slabs at equivalent locations. This enables comparison of the results obtained on the slide side with those obtained on the non-slide side. The graph on the left in Figure 12 shows the results obtained above the impact point and the one on the right below the impact point. The dashed lines represent again the results measured on the slide side of the slabs. On average, the maximum values on the slide side were 81.7 % higher than on other side in the lower velocity test with 20° inclination angle. The corresponding values for the higher velocity tests were 57.9 % and 18.5 % with inclination angles of 10° and 20°.

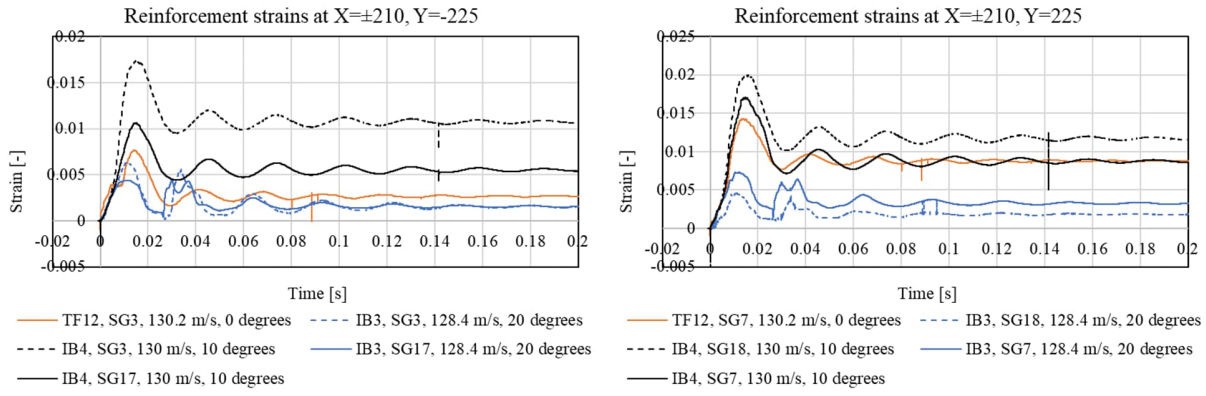

Figure 12. Rear surface horizontal reinforcement strains at X=±210 mm and Y=-225 mm (left) and Y=225 mm (right).

Location X=±210 mm and Y=±225 also enables comparison of the results obtained at equivalent locations above and below the impact location, presented in Figure 13 for the higher velocity tests. The results shown on the left are obtained on the slide side of the slab. The curves obtained above (solid line) and below (dashed line) the centre point are in remarkable agreement. More variation can be observed on the non-

slide side shown on the right. The strains measured at equivalent locations at opposite sides of the slab can generally be almost identical but in some other cases vary considerably. One possible explanation for this is formation of heavy local dents on the relatively small rebars with dense spacing and shear reinforcement. This local denting was not studied in these tests but it has been observed before in similar tests.

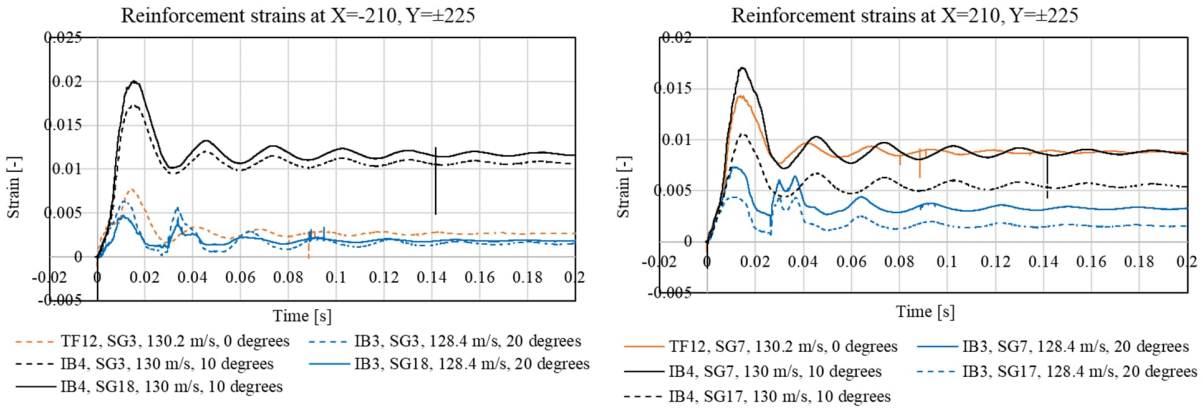

Figure 13. Rear surface horizontal reinforcement strains at X=-210 mm and Y=±225 mm (left) and X=210 mm and Y=±225 mm (right).

The maximum strains decreased in the higher velocity tests when the inclination angle was increased from 10° to 20° with the median decrease being 48% across 20 locations. The maximum strains increased when the inclination angle was increased from 0° to 10° with the median increase being 38% across 13 locations. Again, part of this increase can be attributed to higher concrete stress in the test with 0° inclination angle. The maximum strains decreased in the lower velocity tests when the inclination angle was increased from 0° to 10° with the median decrease being 48% across 11 locations.

CONCLUSIONS AND DISCUSSION

The results of the inclined impact tests suggest that the severity of the impact depends on whether the projectile starts sliding on the impacted surface or not. This in turn depends on the inclination angle and the friction coefficient between the impacting projectile and the impacted surface. For a deformable steel pipe impacting against concrete surface this angle was between 10° and 20°. The difference between the target responses obtained with these angles was notable. The angle when sliding is initiated in an actual aircraft crash should of course be studied separately.

The measured results show that the response of the slab on the side into which the projectile is bound to slide, are larger than on the opposite side. This applies to both cases in which sliding takes place (IB1, IB3, 20° angle) as well as does not take place (IB2, IB4, 10° angle). The effect on the maximum reinforcement strains is larger than on the maximum displacements.

REFERENCES

Riera, J.D. (1968). “On the Stress Analysis of Structures Subjected to Aircraft Impact Forces”, *Nuclear Engineering and Design*, Vol. 8, 1968, pp. 415-426.

Tarallo, F., Rambach, J. -M. (2013). “Some lessons learned from tests of VTT impact program, Phases I and II,” In *Transactions of SMiRT 22*, San Francisco, California, USA, 2013.

Vepsä, A., Saarenheimo, A., Tarallo, F., Rambach, J.-M., Orbovic, N. (2011). “IRIS_2010 –Part II: Experimental Data,” In *Transactions of SMiRT 21*, New Delhi, India, 2011, paper 520.